We are IntechOpen,
the world's leading publisher of
Open Access books
Built by scientists, for scientists

4,800
Open access books available

122,000
International authors and editors

135M
Downloads

Our authors are among the

154
Countries delivered to

TOP 1%
most cited scientists

12.2%
Contributors from top 500 universities

CLARIVATE ANALYTICS
BOOK
CITATION
INDEX
INDEXED

WEB OF SCIENCE™

Selection of our books indexed in the Book Citation Index
in Web of Science™ Core Collection (BKCI)

Interested in publishing with us?
Contact book.department@intechopen.com

Numbers displayed above are based on latest data collected.
For more information visit www.intechopen.com

Indium-Containing Visible-Light-Driven (VLD) Photocatalysts for Solar Energy Conversion and Environment Remediation

Xiangchao Zhang, Duan Huang, Kaiqiang Xu, Difa Xu, Fang Liu and Shiying Zhang

Additional information is available at the end of the chapter

Abstract

Indium-containing visible-light-driven (VLD) photocatalysts including indium-containing oxides, indium-containing sulfides, indium-containing hydroxides, and other categories have attracted more attention due to their high catalytic activities for oxidation and reduction ability under visible light irradiation. This chapter will therefore concentrate on indium-containing nano-structured materials that demonstrate useful activity under solar excitation in fields concerned with the elimination of pollutants, partial oxidation and the vaporization of chemical compounds, water splitting, and CO_2 reduction processes. The indium-containing photocatalysts can extend the light absorption range and improve the photocatalytic activity by doping, heterogeneous structures, load promoter, and morphology regulation. A number of synthetic and modification techniques for adjusting the band structure to harvest visible light and improve the charge separation in photocatalysis are discussed. In this chapter, preparation, properties, and potential applications of indium-containing nano-structured materials used as photocatalysis will be systematically summarized, which is beneficial for understanding the mechanism and developing the potential applications.

Keywords: photocatalysis, visible-light-driven (VLD), indium-containing, solar energy conversion, environment remediation

1. Introduction

The current rapid industrial development causes the serious energy and environmental crises. Since Fujishima [1] reported the photocatalytic activity of TiO_2, the research enthusiasm has not diminished. Semiconductor photocatalysis has received much attention as a potential solution to the worldwide energy shortage and for counteracting environmental degradation. Photocatalysis is a light-driven chemical process over the surface of photocatalyst that can produce hydrogen from water, convert solar energy into electric energy, degrade organic pollutants, and reduce CO_2 into organic fuels [2]. Photocatalyts provide a potential strategy to solve these problems because these materials not only convert solar energy directly into usable or storable energy resources, but can also decompose organic pollutants under solar-light irradiation [3–9].

Over the past several years, researchers have made considerable effort to increase the visible-light-driven (VLD) photocatalytic activity of the photocatalysts [10, 11]. There are two strategies employed in the design of the VLD photocatalysts. One is the chemical modifications on a UV-active photocatalyst, including doping of foreign elements or coupling with a narrow band gap semiconductor. In order to extend the absorption of light into the visible region, three approaches have been widely used on semiconductors: (I) modification of the VB, (II) adjustment of the CB, and (III) continuous modulation of the VB and/or CB (see **Figure 1**) [12]. The other is to develop novel photocatalysts with VLD photocatalytic activity. The development of photocatalysts under visible light irradiation is one of the major goals for enhancing the efficient utilization of solar energy and realizing practical industrialization.
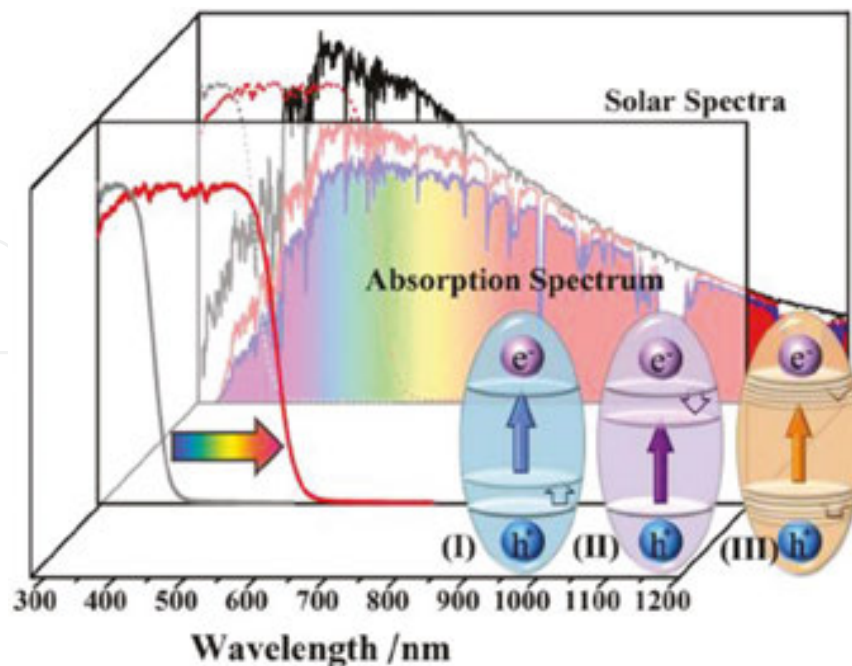

Figure 1. Three strategies to narrow the band gap of semiconductor photocatalysts to match the solar spectrum [12].

Recently, photocatalysis driven by visible light has gained great attention, as the visible light occupies most part of the solar spectrum such as: bismuth compounds (Bi_2WO_6 [13], Bi_2MoO_6 [14], $BiVO_4$ [15], $BiOBr$ [16]), silver compounds($AgAlO_2$ [17], Ag_2CrO_4 [18], Ag_2CO_3 [19], $AgVO_3$ [20], Ag_3PO_4 [21]), and indium compounds(In_2O_3 [22], $CaIn_2O_4$ [23], $InVO_4$ [24], In_2S_3 [25]). Up to now, much attention has been given to a series of visible light active indium compound. The In 5s orbital in the valence band of the semiconductor may hybrid with O 2p or S 2p orbital to form a new energy level, which could narrow the band gap of the indium compound and enhance the photocatalytic activity with the visible light irradiations [26]. Many novel indium-containing VLD photocatalysts were reported. Herein we review the fundamental challenges and recent progress on indium-containing VLD photocatalysts.

Starting with a brief introduction, we will give an overview on the development of high-efficiency, indium-containing VLD photocatalysts. Section 2 covers indium-containing oxides including single-metal oxide (In_2O_3), double-metal containing indium oxides $A_xB_yO_z$ (A site containing indium compounds $InMO_4$ (M=V, Nb, Ta), B site containing indium compounds $AInO_2$ (A=Ag, Na, Li), MIn_2O_4 (M = Ca, Sr, Ba). Section 3 describes systems involving indium based sulfides such as single-metal sulphide (In_2S_3), double-metal containing indium sulfides AIn_xS_y (A=Na, Cu, Ag, Cd, Zn), and containing indium solid solution ZnS-CuInS$_2$-AgInS$_2$, $(CuIn)_xZn_{2(1-x)}S_2$. Indium-containing hydroxides will be discussed in section 4. A number of synthetic and modification techniques for adjusting the band structure to harvest visible light and improve the charge separation in photocatalysis are discussed. A comparative analysis of the systems discussed and their future projection as environmentally friendly photocatalytic systems will conclude the review. Finally, some feasible ways to design and improve the visible-light responding photocatalysts are concluded, and the development of indium-containing oxides semiconductor photocatalysts is also proposed.

The application of indium-containing VLD photocatalysts for solar energy conversion and environment remediation as an important challenge will be listed. We aim to put together the research effort having been made so far, with a view of providing a good reference and inspiring new ideas for tackling this important challenge. In this chapter, preparation, properties, and potential applications of indium-containing nano-structured materials used as photocatalysts will be systematically summarized, which is beneficial for mechanism understanding and developing potential applications.

2. Indium-containing oxides

2.1. Indium oxide

Recently, the reported research has investigated In_2O_3 in an attempt to develop novel photocatalysts for water splitting. In_2O_3 fulfils some important requirements for the direct photo electrolysis of water such that the position of the conduction and valence band edges bracket the radix potentials of water, and In_2O_3 has an excellent conductivity and stability. In_2O_3 generally exists in two forms: cubic (C-In_2O_3) and hexagonal (H-In_2O_3). Currently, there are reports on the morphology of In_2O_3 mostly in the cubic structure of C-In_2O_3 and a few hexagonal structure of H-In_2O_3. So far, researchers have successfully synthesized the In_2O_3

with various morphology such as particles [27], fibers [28], porous particles [29], and cubes of nanostructures [30]. **Figure 2** shows the SEM images of In₂O₃ nanostructures with different morphologies.
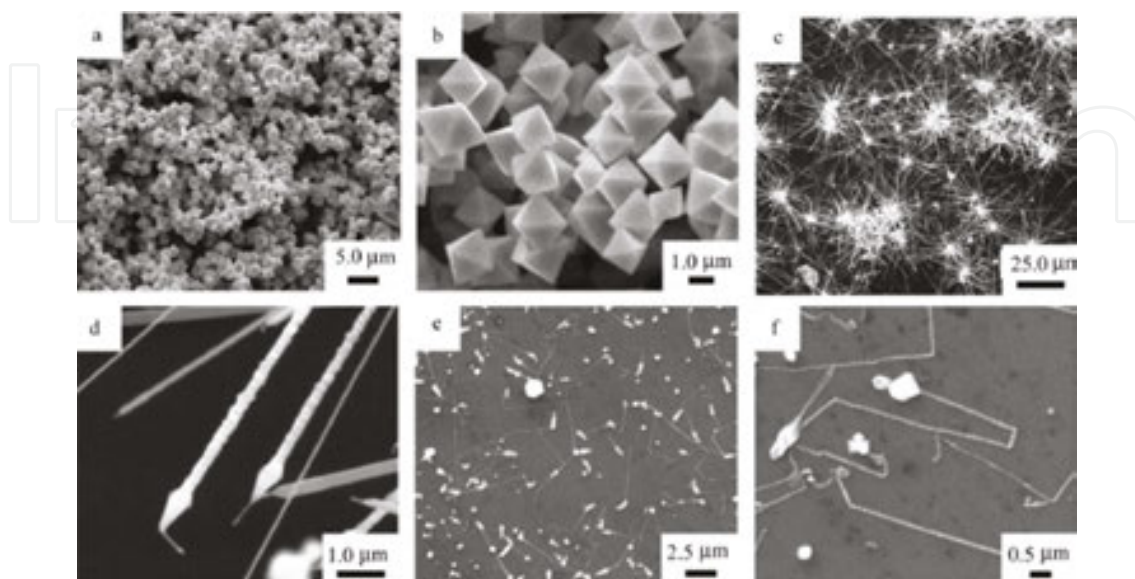

Figure 2. SEM images of In$_2$O$_3$ nanostructures with different morphologies synthesized at 800℃ for 1 h: a, b-octahedrons; c, d-nanobelts and dentate nanowires; e, f-nanocrystal chains [31].

In$_2$O$_3$ is transparent to visible light because of its wide band gap (E_g=3.55-3.75 eV) [31], which decreases its potential efficiency for water splitting under solar illumination. In$_2$O$_3$ was modified by various methods. The results showed that the modified In$_2$O$_3$ have better response in the visible light region and have higher photocatalytic activity than In$_2$O$_3$. For example, Karla et al. [32] reported that N-doped In$_2$O$_3$ were prepared and found that the rate of decomposition of water under visible light has improved compared with pure In$_2$O$_3$. Compared to ion doping methods, constructing compound semiconductor heterojunction broaden the optical response range and effectively, the separation of electrons and holes. Li et al. [33] successfully synthesized heterojunction CuO/In$_2$O$_3$ composite photocatalysts by hydrothermal method. Under visible light, Rhodamine B as the target pollutants examined the catalytic properties of the composite photocatalysts and found its catalytic activity much higher than pure In$_2$O$_3$. The enhanced photocatalytic activity is due to the CuO and In$_2$O$_3$ forming heterogeneous structures, which can effectively improve the separation efficiency of the light-generated charge and extend the light absorption range. For solid solutions consisting of Ga$_2$O$_3$ and In$_2$O$_3$, Ga$_{1.14}$In$_{0.86}$O$_3$ showed the highest photocatalytic activity for H$_2$ evolution from aqueous methanol solutions and for O$_2$ evolution from aqueous silver nitrate solutions. In comparison, the solid solutions of Y$_2$O$_3$ and In$_2$O$_3$, Y$_{1.3}$In$_{0.7}$O$_3$, showed the highest photocatalytic activity for the overall water splitting when combined with RuO$_2$ as a promoter.

So far, the preparation methods of In$_2$O$_3$ mainly are thermal evaporation (TE) [34], chemical vapour deposition (CVD) [35], laser ablation (PLD) [36], metal organic chemical vapour deposition (MOCVD) [37], and a variety of wet chemical methods [38–40]. Among them, the

characteristic of wet chemical method is the lowest preparation temperature, but their degree of crystallinity is poor; their morphology is mainly nanowire hexagonal structure, nanoparticles, and squares. In addition to the main method as described above, preparation cubic In_2O_3 by processing the precursor material is also suffering much attention [41–43].

2.2. Double-metal containing indium oxides

Double-metal containing indium oxides ($A_xB_yO_z$) due to the different site of element In position (A or B bits), can be divided into two categories: A site containing indium compounds $InMO_4$(M=V, Nb, Ta), B site containing indium compounds $AInO_2$ (A=Ag, K, Na, Li), MIn_2O_4 (M = Ca, Sr, Ba).

2.2.1. A site containing indium oxides

$InMO_4$ (M = V, Nb, Ta) compounds belong to ABO_4 compound, where In is in A bit. Their crystal structures were: $InNbO_4$ ($InTaO_4$) belong to monoclinic system with octahedral InO_6 and NbO_6 (TaO_6); $InVO_4$ belongs to orthorhombic system with octahedral InO_6 and tetrahedral VO_4. $InTaO_4$ was 5d compound (E_g = 2.6 eV), $InNbO_4$ was 4d compound (E_g = 2.5 eV), and $InVO_4$ was 3d compound (E_g = 2.0 eV), bandgap of the $InMO_4$ compound with M from 5d Ta to 4d Nb to 3d V reduced [44]. Song et al. [45] prepared one-dimensional $InVO_4$ nanofibers with width of 30-100 nm under visible light illuminated through 6 h, wherein the nitrobenzene degradation reached 69%. Zou [46] prepared $InMO_4$ (M = Nb^{5+}, Ta^{5+}) by high-temperature solid phase method. Under visible light (λ > 420 nm) irradiation, the hydrogen production rate of $InMO_4$ (M = Nb^{5+}, Ta^{5+}) is that of P25, 4.0 and 3.5 times, respectively. Meanwhile, the $InMO_4$ (M = V, Nb, Ta) photocatalysts were modified by doping heterogeneous structures method. The results showed that visible light absorption and photocatalytic activity of $InVO_4$ after modification had been enhanced [47, 48]. Zhang et al. [49] prepared graphene (Gr)/ $InNbO_4$ composite photocatalysts by hydrothermal method from which the apparent rate constant of (0.0346 min^{-1}) degradation MB is higher than pure $InNbO_4$ (0.0185 min^{-1}) under visible light illumination.

$InVO_4$, due to suitable conduction band can be a promising photocatalyst for H_2 production under visible light irradiation. In addition, there are many reports indicating that the desired morphology and size of photocatalysts could regulate the position of the energy band to achieve higher radix ability. Yan et al. [50] reported that the nanosized $InVO_4$ nanoparticles with the size of 20 nm showed higher photocatalytic activity of H_2 production than $InVO_4$ microspheres. Hu et al. [51] synthesized g-C_3N_4/nano-$InVO_4$ heterojunction-type photocatalysts by in situ growth of $InVO_4$ nanoparticles onto the surface of g-C_3N_4 sheets via hydrothermal process. The formation of interfaces could promote the charge transfer and inhibit recombination of charge-hole pairs, which significantly improved the photocatalytic activity of H_2 evolution of 212 μmol/g·h from water-splitting. **Figure 3** is a schematic illustration of g-C_3N_4/$InVO_4$ composite under visible light irradiation.

Currently, these are the following methods for synthetic $InVO_4$: solid-phase synthesis [52], which is difficult to obtain a large surface area, pore volume, and a high mesoporous materi-

als; mesoporous $InVO_4$ obtained by sol-gel method [53] are disorderly, has wide pore size distribution, pore walls were generally amorphous, and with poor thermal stability; surfactant templating method [54] can obtain larger surface area mesoporous $InVO_4$, but the manufacturing process requires high temperatures and the morphology is irregular.
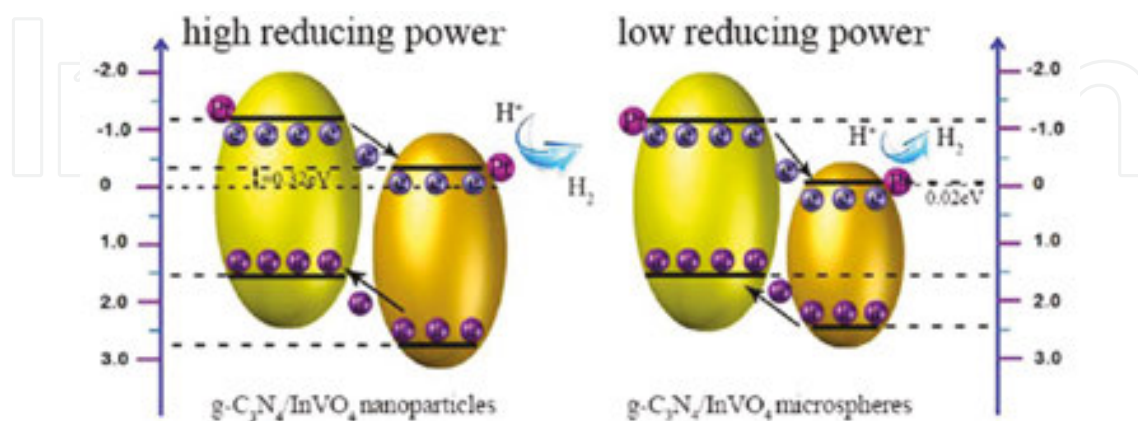

Figure 3. Schematic illustration of g-C_3N_4/$InVO_4$composite under visible light irradiation [51].

2.2.2. B site containing indium oxides

Photochemical dye degradation has been limited by the efficiency of the catalyst materials with respect to photon absorption. An ideal catalyst would be capable of using as much of the solar spectrum as possible, in particular the visible region. As we know, delafossites structure of materials have the potential to provide this photoactivity. These materials have the general formula ABO_2 and are based on the mineral $CuFeO_2$, also known as delafossite. $AInO_2$ (A = Ag, K, Na, Li) belong to ternary oxide ABO_2, where In is in B bit. Crystal structure of $AgInO_2$, $LiInO_2$ and $NaInO_2$ are delafossite, α-$LiFeO_2$ and α-$NaFeO_2$, respectively. The band gap values of $AgInO_2$, $LiInO_2$ and $NaInO_2$ are 2.0eV, 3.7eV and 3.9eV, respectively. These materials share the ability to alter the band structure by using chemical substitution. In particular, substitution on the B-site in these materials can be used to tune the physical properties of delafossites for specific applications. $AgInO_2$ is a narrow bandgap semiconductor material which responds in the visible light range. Wang et al. [55] reported 0.5 wt% Pt/$NaInO_2$ can completely degrade MB in 1h. Jonathan et al. [56] reported the effect of electronic structure changes in $NaInO_2$ and $NaIn_{0.9}Fe_{0.1}O_2$ on the photo reduction of Methylene Blue. **Figure 4** shows the (A) crystal structure, (B) diffuse reflectance spectroscopy, and (C) energy level diagram of the $NaInO_2$ and $NaIn_{0.9}Fe_{0.1}O_2$, respectively. Diffuse reflectance spectroscopy was used to determine the band gap values of 3.9 eV and 2.8 eV for $NaInO_2$ and $NaIn_{0.9}Fe_{0.1}O_2$, respectively. Energy level diagram describing the flat band (EFB; dashed line), conduction band (ECB), and valence band (EVB) potentials of TiO_2, $NaInO_2$, and $NaIn_{0.9}Fe_{0.1}O_2$ in relation to some relevant electrochemical radix couples; potentials are in the reversible hydrogen electrode (RHE) scale (b). The spread in CB and VB potentials represents the experimental uncertainty in band edge determination.
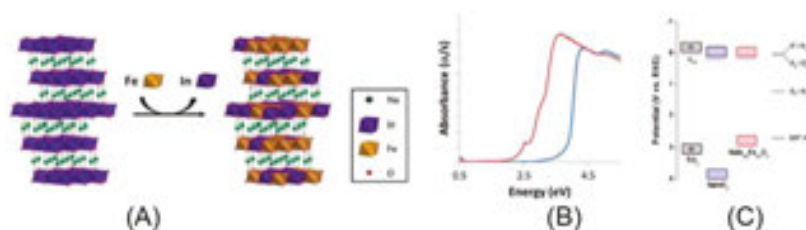
Figure 4. (A) Rhombohedral crystal structure,(B) Diffuse reflectance spectroscopy, and (C) Energy level diagram of the $NaInO_2$ and $NaIn_{0.9}Fe_{0.1}O_2$ [56].

MIn_2O_4 (M = Ca, Sr, Ba) belongs to the family of ternary oxide AB_2O_4, where In is in B bit. Their crystal structures are: $CaIn_2O_4$ and $SrIn_2O_4$ having the same octahedral InO_6 network structure, and $BaIn_2O_4$ having a more complex polyhedron InO_x structure. Sato and Tang team synthesized a series of photocatalysts MIn_2O_4 (M = Ca, Sr, Ba) and studied the crystal and electronic structure of the photocatalysts relationship with their visible light photocatalytic activity. Sato group [57] found that different crystal structures of MIn_2O_4 (M = Ca, Sr, Ba) have an impact on their photocatalytic activity. The crystal structures of $CaIn_2O_4$ and $SrIn_2O_4$ are orthorhombic and $BaIn_2O_4$ was monoclinic. The order of catalytic activity of water splitting in the xenon lamp irradiation were: $CaIn_2O_4 > SrIn_2O_4 > BaIn_2O_4$. Tang et al. [58] prepared MIn_2O_4 (M = Ca, Sr, Ba) by solid phase methods. They fall in the visible order solution MB catalytic activity were: $CaIn_2O_4 > SrIn_2O_4 > BaIn_2O_4$, wherein $CaIn_2O_4$ showed the highest activity (**Figure 5**). The reason of the order activity is that mesh structure of $CaIn_2O_4$ and $SrIn_2O_4$ helps photogenerated electron transfer. Inoue et al. [59] investigated the photocatalytic properties for water decomposition of alkali metal, alkaline earth metal, and lanthanum indates with an octahedrally coordinated In^{3+} d10 configuration ion. The photocatalytic activity for water decomposition under UV irradiation was considerably large for RuO_2-dispersed $CaIn_2O_4$, $SrIn_2O_4$, and $Sr_{0.93}Ba_{0.07}In_2O_4$ but very poor for RuO_2-dispersed $AInO_2$ (A = Li, Na) and $LnInO_3$ (Ln = La, Nd). The geometric structures of the InO_6 octahedral units for these indate were compared. As shown, the photo-catalytic active indates possessed distorted InO_6 octahedral with dipole moments. The internal fields that arose due to the dipole moment promoted the charge separation in the initial process of photo-excitation.
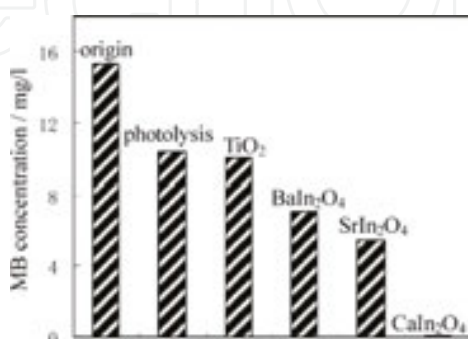

Figure 5. MB original concentration, MB photolysis and its concentration variation after 120 min visible light irradiation ($\lambda > 420$ nm) on the different oxides [58].

3. Indium-containing sulfide

Indium based sulphides include single-metal sulfide (In_2S_3), double-metal containing indium sulfides AIn_xS_y (A = Na, Cu, Ag, Cd, Zn), and containing indium solid solution ZnS-CuInS$_2$-AgInS$_2$, $(CuIn)_xZn_{2(1-x)}S_2$. Compared with indium-containing oxides, Indium based sulphides has narrow band gap which can make good use of visible light and have been extensively studied. But its low stability, prone to light decay, and other shortcomings limit its further application.

3.1. Indium sulfide

In_2S_3 have three different forms of structural defects: α-In_2S_3(defect cube), β-In_2S_3(defect spinel, cubic, or tetragonal structure), and γ-In_2S_3 (layered hexagonal). The band gap of In_2S_3 is E_g=1.9-2.3 eV [60], and it belongs to the n-type narrow band gap semiconductor. Researchers mostly used solvothermal or hydrothermal methods to prepare excellent performance of visible light photocatalyst In_2S_3. Liu et al. [61] prepared tetragonal β-In_2S_3 nanotube by solvothermal method. The nanotube with diameter of about 10-20 nm, pipe wall thickness of 2 nm, tube length 1μm, and under simulated sunlight degraded Rhodamine with high rate. In addition, the researchers have further explored In_2S_3, such as the following: (1) the relationship between crystal or precious metal co-catalyst species and the catalytic activity and selectivity of light catalysis: Xing et al. [62] prepared a heterogeneous structure photocatalyst In_2S_3/g-C_3N_4 by hydrothermal method and they found 40 wt% In_2S_3/g-C_3N_4 degradation RhB rate in 30 min, can be 96% under visible light (λ > 420 nm) irradiation, far higher than the 50% of pure In_2S_3; (2) the relationship between crystal or precious metal co-catalyst species: Fu et al. [63] reported the preparation of the tetragonal and cubic phases In_2S_3 by hydrothermal method, both of their photocatalytic hydrogen production under visible light were investigated (**Figure 6**). The results showed that ordered tetragonal In_2S_3 has no hydrogen production activity, while disordered cubic structure In_2S_3 showed stable photocatalytic hydrogen production activity. At the same time, the authors also investigated the effect of precious metal as co-catalyst on the order photocatalytic activity of In_2S_3 and results are: Pd>Pt>Ru>Au; (3) the catalytic activity and selectivity of light catalysis: Xie et al. [64] used the microspheres In_2S_3 prepared by hydrothermal method, with selective degradation using 41.4% benzyl alcohol in 4 h invisible light.

Currently, researchers have explored a variety of ways for preparing In_2S_3 with different morphology. For example: Afzaal et al. [65] used high temperature vapour deposition to get In_2S_3 nanorods on a glass substrate. Liu et al. [66] used indium nitrate as an indium source, dodecyl mercaptan as a sulfur source to synthesis β-In_2S_3 nanotube structure with nanotube length of 1-10 μm, and width less than 15 nm by pyridine solvent thermal reaction method. Son et al. [67] reported the use of $InCl_3 \cdot 4H_2O$ and elemental sulfur as a precursor with a certain proportion of the oleylamine oil, then obtained hexagonal indium sulfide nanosheets with thickness of 0.76 nm. In addition, the researchers also used the hot water or solvent hot methods for preparing a variety of three-dimensional structures In_2S_3, such as flower microspheres [68], hollow microspheres [69], and dendrites [70].
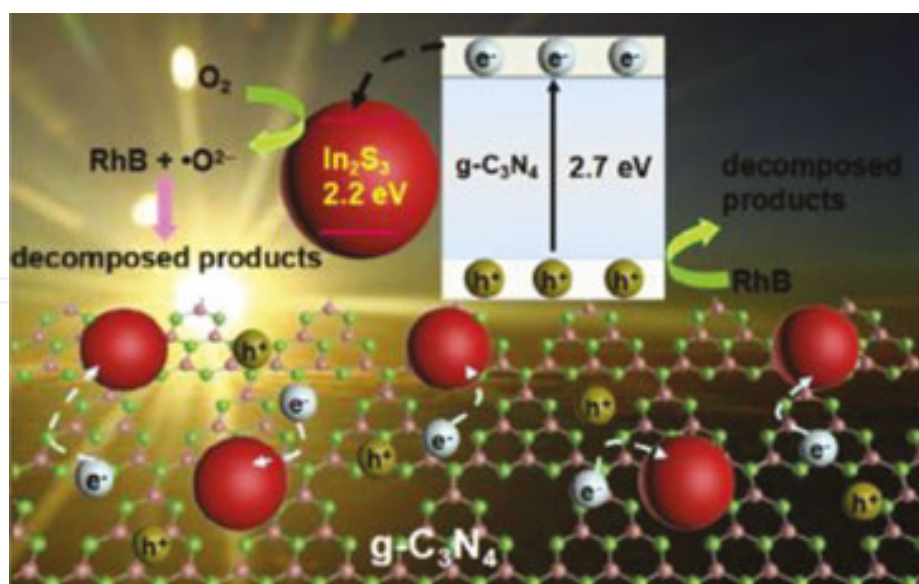
Figure 6. Schematic illustration of the In_2S_3/g-C_3N_4 photocatalytic reaction process under visible light irradiation [62].

3.2. Double-metal containing indium sulfide

The band gap of double-metal containing indium sulphides AIn_xS_y (A = Na, Cu, Ag, Zn) range from 1.87 to 2.5eV which have light response in the visible light. In recent years, the AIn_xS_y as visible light catalyst have been extensively studied with focus mainly on $ZnIn_2S_4$.

$ZnIn_2S_4$ is a II-III-VI family ternary metal sulfides with hexagonal and cubic spinel structure and have narrow band gap (E_g = 2.1-2.4 eV). $ZnIn_2S_4$ has strong light absorption in the visible region which is worth studying as a visible light catalyst. Li et al. [71] were first using $ZnIn_2S_4$ on visible light catalytic hydrogen. Hexagonal $ZnIn_2S_4$ (space group P3m1) is a typical layered compound and the band gap is about 2.4 eV (CB: –0.29 eV vs NHE; VB: 2.11 eV vs NHE) which have a strong and appropriate response on visible light. Li et al. [72] prepared cubic $ZnIn_2S_4$ nanoparticles and hexagonal phase $ZnIn_2S_4$ microspheres by changing the indium precursor and then investigated two crystal phases $ZnIn_2S_4$ degrade methyl orange in visible light. The results showed cubic phase $ZnIn_2S_4$ having activity just at the beginning, while the hexagonal phase has shown a high catalytic activity.

Researchers modified $ZnIn_2S_4$ to further improve its photocatalytic activity by means of ion doping and semiconductor composite. Wen-Hui Yuan group [73] first reported that doping N can improve visible light photocatalytic activity of $ZnIn_2S_4$ degradation of MB. Shen et al. [74] reported composite photocatalysts Cu-$ZnIn_2S_4$ have higher visible light catalytic activity than pure $ZnIn_2S_4$ (**Figure 7**).

So far, the preparation methods of $ZnIn_2S_4$ mainly are: chemical precipitation method [75], precursor route [76], hydrothermal method [77], microwave-hydrothermal method [78], solid phase method [79], the template [80], and so on. Among them, the hydrothermal method is the typical preparation method, which is more beneficial to controlling the different morphologies of $ZnIn_2S_4$.
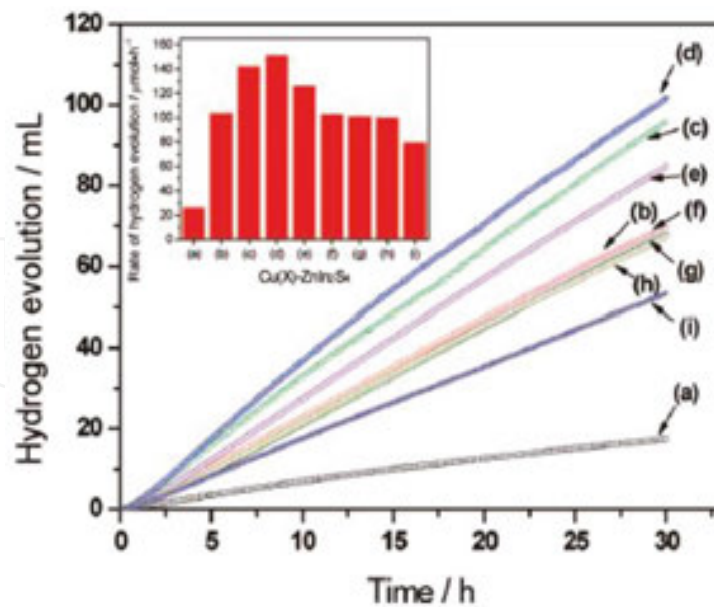
Figure 7. Hydrogen production under visible-light irradiation over Cu(X)-ZnIn$_2$S$_4$; the values of X were (a) 0.0 wt%, (b) 0.1 wt%,(c) 0.3 wt%, (d) 0.5 wt%, (e) 0.7 wt%, (f) 0.9 wt%, (g) 1.2 wt%, (h)1.6 wt%, (i) 2.0 wt%[74].

CdIn$_2$S$_4$ also is a kind of II-II-VI family ternary metal sulphides, its band gap E$_g$=2.12-2.29 eV [81]. Researchers prepared different morphologies CdIn$_2$S$_4$ by different methods and studied their visible light photocatalytic activity. Bhirud et al. [81] prepared different morphologies CdIn$_2$S$_4$. When not added, the active agent was flower shape; adding a surfactant polyvinyl-pyrrolidone was double cone; adding a surfactant CTAB was hollow spheres. Three differ-ent morphologies CdIn$_2$S$_4$ catalysed water splitting under visible light have shown different catalytic activity and double cone is the highest (3238 μmol. (g.h)$^{-1}$). Mu et al. [82] prepared spherical particles CdIn$_2$S$_4$ with average size of 236 nm from which degradation rate for methyl orange is 98% in the visible light illumination.

=2.12-2.29 eV [56AgIn$_x$S$_y$ include AgInS$_2$ and AgIn$_5$S$_8$. AgInS$_2$ has chalcopyrite (t-AgInS$_2$) and orthogonal (o-AgInS$_2$) two crystal phases and the band gap values respectively were 1.87 and 1.98 eV [83, 84]; AgIn$_5$S$_8$ is cubic crystalline phase (c-AgIn$_5$S$_8$) and its the band gap value is 1.7-2.0 eV [85]. Both of the degrading organic substances under visible light irradiation exhibited good photocatalytic properties [86, 87]. NaInS$_2$ belongs to a narrow band gap semiconductor material (E$_g$ = 2.3 eV) [88]. Researchers applied hydrogen production and degradation of organic pollutants under visible light [88, 89].

3.3. Solid solution containing indium sulfide

Solid solution containing indium adjust the content of the different components of the solid solution to achieve the band gap of a solid solution of regulation. For now, there are reports of solid solution system ZnS-CuInS$_2$, ZnS-AgInS$_2$, and ZnS-AgInS$_2$-CuInS$_2$. In this regard, Kudo teams have done a lot of research. Tsuji group [90, 91] used ZnS and narrow bandgap CuInS$_2$ or AgInS$_2$ by calculating to form a visible light catalyst (CuIn)$_x$Zn$_{2(1-x)}$S$_2$, (AgIn)$_x$Zn$_{2(1-x)}$S$_2$, and ZnS-CuInS$_2$-AgInS$_2$. Guo [92, 93] prepared (CuIn)$_x$Zn$_{2(1-x)}$S$_2$ (x = 0.01–0.5) solid solution

using CTAB as surfactant by hydrothermal method. Compared with the method used by Kudo group, their method has no calcination and the products have smaller particle size. Studies have shown that with the increase of x value, the absorption band edge of $(CuIn)_xZn_{2(1-x)}S_2$ became obvious red shift and the composition of the solid solution have great influence on hydrogen production performance (**Figure 8**).
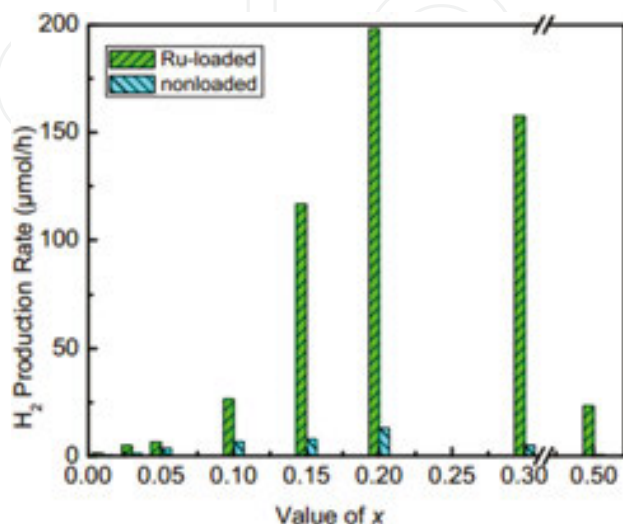

Figure 8. The photocatalytic hydrogen production activities of $(CuIn)_xZn_{2(1-x)}S_2$ solid solutions under visible-light irradiation [92].

In recent years, containing indium solid solution has made great progress in China. Guijun Ma [94] who belongs to CAS Dalian Institute of Physical Chemistry used solvothermal method to synthesize $CuInS_2$-ZnS solid solution. Compared with the results of Kudo, their products have smaller particle size (average particle size 30-50 nm) and exhibit stable photocatalytic hydrogen production. Chen et al. [95, 96] from Harbin Institute of Technology synthesized nano-porous solid solution photocatalysts ZnS-In_2S_3-Ag_2S and ZnS-In_2S_3-CuS by self-assembled solvothermal method. Under visible light, the photocatalysts exhibit excellent photocatalytic hydrogen performance and the apparent quantum yield is 19.8% and 22.6%, respectively.

Kudo et al. [97] synthesized $(AgIn)_xZn_{2(1-x)}S_2$(x = 0.17–0.5) solid solutions. The band gaps can be tuned from 2.40 to 1.95 eV, which lie between that of ZnS and $AgInS_2$ (**Figure 9A**). The intensive absorption bands with steep edges of the doped ZnS photocatalysts indicate that the visible light absorption was due to the band transition instead of the transition from impurity levels to the conduction band of ZnS. DFT calculations revealed that the valence band of it is mainly composed of hybrid orbitals of S 3p and Ag 4d, and the conduction band is composed of hybrid orbitals of In 5s5p +Zn 4s4p in $(AgIn)_xZn_{2(1-x)}S_2$ solid solution, which is located between those of ZnS and $AgInS_2$ (**Figure 9B**). The photocatalytic activity is greatly dependent on the composition and the Pt (3 wt%) loaded. $(AgIn)_{0.22}Zn_{1.56}S_2$ photocatalyst exhibited the highest activity for H_2 evolution in the presence of sacrificial reagent under visible light irradiation ($\lambda > 420$ nm); the quantum yield of the samples was as high as 20% at 420 nm.
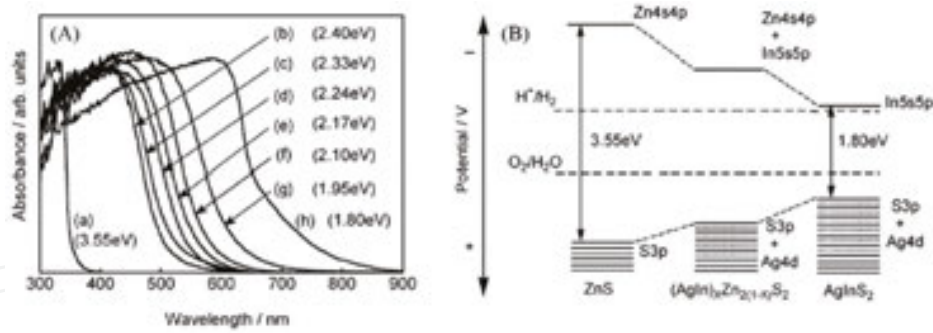
Figure 9. (A) Diffuse reflection spectra of $(AgIn)_xZn_{2(1-x)}S_2$ solid solutions; the values of x are (a) 0, (b) 0.17, (c) 0.22, (d) 0.29, (e) 0.33, (f) 0.40, (g) 0.5, and (h) 1. (B) Band structures of $(AgIn)_xZn_{2(1-x)}S_2$ solid solutions, ZnS and $AgInS_2$[97].

4. Indium-containing hydroxides

Indium-containing hydroxides include $In(OH)_3$ and $InOOH$. The band gap values were 5.15 eV and 3.70 eV respectively [98], and they belongs to the wide band gap semiconductor photocatalyst.

$In(OH)_3$ is a very important n-type photocatalyst and its crystal structure is: per In^{3+} ions with six OH^- ions constituting the octahedral structure and $In(OH)_3$ belongs to wide-band gap light catalyst which does not respond in the visible light range. The researchers modified it to try to expand its range of light absorption by a variety of methods. For example, Lei et al. [99] synthesized photocatalyst $In(OH)_yS_z$ by hydrothermal method. The result is that the absorption edge of $In(OH)_3$ followed S^{2-} substituted with OH^- moved from 240 nm to 570 nm (**Figure 10**).

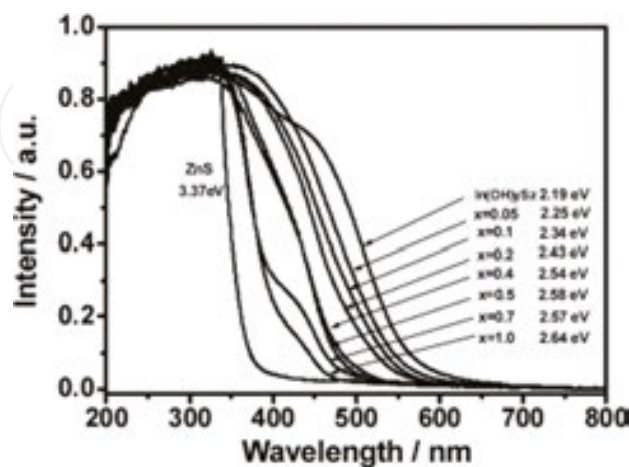**Figure 10.** DRS of ZnS, $In(OH)_yS_z$ and $In(OH)_yS_z$:Zn catalysts with different X value (X denotes the atomic ratio of Zn/In in the synthesis solution). The $In(OH)_yS_z$ and $In(OH)_yS_z$:Zn were obtained with atomic ratio of S/In = 2.0 [99].

InOOH is orthorhombic crystal, compared with the crystal structure of $In(OH)_3$, InOOH can be seen as distorted octahedral InO_6 co-built by the edge of the way. Researchers, through the composite doping methods such as wide band gap photocatalyst InOOH modified to the scope and the absorption of visible light photocatalytic activity. Song et al. [100] prepared porous carbon spheres/InOOH composite photocatalyst by in-situ reaction. Compared with the pure InOOH, the composite photocatalyst of optical absorption edge had undergone a drastic red shift and improved the visible light photocatalytic activity. Ge et al. [101] reported that N, C doping InOOH has a response in the visible light range due to the doping, and narrowing of the band gap of InOOH (**Figure 11**).
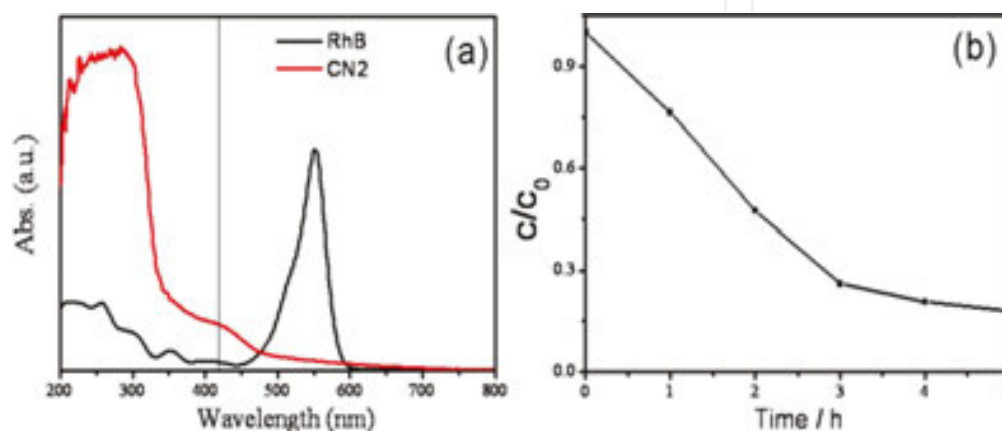

Figure 11. Comparison of UV-vis diffuse reflectance spectral of CN_2 and RhB (a) and the photo degradation efficiencies of RhB by 0.1 g of CN_2 under monochromatic light source (λ= 420 nm) (b). C_0 and C are the initial concentration after the adsorption equilibrium and temporal concentration of RhB at different times, respectively [101].

5. Conclusion and prospective

The use of semiconductor materials photocatalytic degradation organic pollutants and producing hydrogen has very important significance for environmental management, and energy depletion. However, the low visible light catalytic efficiency has hampered the development of photocatalytic technology. There is an urgent task in developing new and efficient visible light catalytic system.

In summary, the indium-based photocatalytic materials have good visible response and strong visible light photocatalytic activity and possess broad prospects on photocatalytic water environment, capacity, and other degradation of organic pollutants. The current findings indicate that photocatalytic activity of indium-based photocatalysts is affected by its size, morphology, and crystal structure; doping, heterogeneous structures, load promoter, and morphology regulation methods can extend the light absorption range and improve the photocatalytic activity. Indium-based photocatalysts also have the following problems which needs to do further exploration and research:

1. At the moment, researches of indium-based photocatalysts mainly focus on degradation of organic compounds and hydrogen production with little research for CO_2 reduction, which may be the weakness of reducing capacity. Using widely the photocatalysts on CO_2 reduction by various channels to improve their reducing ability is needed.

2. Indium-based photocatalyst of electron transfer mechanism, carrier generation and recombination, free radical generation and detection, and photocatalytic mechanism of research reports is little and this may require deeper and more systematic research and inspection.

3. So far, the reports on some narrow band gap and good photoelectric properties of indium-based photocatalysts application on the visible light catalysis have not appeared yet. For example, InN ($E_g = 0.7$ eV) [102].

4. Finally, the high cost for all indium-based compound limited its large-scale application. Therefore, how to significantly reduce its production cost is an issue to consider.

Acknowledgements

Author details

Xiangchao Zhang[1*], Duan Huang[1,2], Kaiqiang Xu[1,2], Difa Xu[1], Fang Liu[1,2] and Shiying Zhang[1,2*]

*Address all correspondence to: xczhang@ccsu.edu.cn; cszhangsy@ccsu.edu.cn

1 Hunan Province Key Laboratory of Applied Environmental Photocatalysis, Changsha University, Changsha, Hunan, PR China

2 College of Material Science and Engineering, Hunan University, Hunan, PR China

References

[1] Fujishima A, Honda K. Electrochemical photolysis of water at a semiconductor electrode. Nature, 1972, 238(5358):37–38.

[2] Carey J H, Lawrence J, Tosine H M. Photodechlorination of PCB's in the presence of titanium dioxide in aqueous suspensions. Bulletin of Environmental Contamination & Toxicology, 1976, 16(6):697–701.

[3] Matsunaga T, Tomoda R, Nakajima T, et al. Photoelectrochemical sterilization of microbial cells by semiconductor powders. Fems Microbiology Letters, 1985, 29(1–2): 211–214.

[4] Fujishima A, Rao T N, Tryk D A. Titanium dioxide photocatalysis. Journal of Photochemistry & Photobiology C Photochemistry Reviews, 2000, 1(1):1–21.

[5] Farrauto R J, Heck R M. Environmental catalysis into the 21st century. Catalysis Today, 2000, 55:179–187.

[6] Muneer M, Philip R, Das S. Photocatalytic degradation of waste water pollutants. Titanium dioxidemediated oxidation of a textile dye, Acid Blue 40. Research on Chemical Intermediates, 1997, 23(3):233–246.

[7] Asahi R, Morikawa T, Ohwaki T, et al. Visible-light photocatalysis in nitrogen-doped titanium oxides. Science, 2001, 293(5528):269–271.

[8] Li D, Haneda H, Hishita S, et al. Visible-light-driven nitrogen-doped TiO_2 photocatalysts: effect of nitrogen precursors on their photocatalysis for decomposition of gas-phase organic pollutants. Materials Science & Engineering B, 2005, 117:67–75.

[9] Li S, Liao J J, Lin S W, et al. Researches progress on fabrication and doping as well as modification of titania nanotubes. Journal of the Chinese Society, 2011, 39(6):1034–1044. (In Chinese)

[10] Zhao Z Z, Xie Y D, Zhang B, et al. Advances on doped TiO_2 visible light driven photocatalysts. Bulletin of the Chinese Ceramic Society, 2012, 31(1):92–95.

[11] Zhuo W Y, Cao Q Y, Tang S Q, et al. Progress in improving visible light photocatalytic activity of nano-titanium dioxide. Journal of the Chinese Society, 2006, 34(7):861–867. (In Chinese)

[12] Tong H, Ouyang S, Bi Y, et al. Nano-photocatalytic materials: possibilities and challenges. Advanced Materials, 2012, 24(2):229–251.

[13] Ju W, Fang D, Yan Z, et al. Synthesis of Bi_2WO_6 nanoplate-built hierarchical nest-like structures with visible-light-induced photocatalytic activity. Journal of Physical Chemistry C, 2007, 111(34):12866–12871.

[14] Tian G, Chen Y, Zhou W, et al. Facile solvothermal synthesis of hierarchical flower-like Bi_2MoO_6 hollow spheres as high performance visible-light driven photocatalysts. Journal of Materials Chemistry, 2010, 3(3):887–892.

[15] Jiang H, Meng X, Dai H, et al. High-performance porous spherical or octapod-like single-crystalline $BiVO_4$ photocatalysts for the removal of phenol and methylene blue

under visible-light illumination. Journal of Hazardous Materials, 2012, 217–218(6):92–99.

[16] Zhang J, Shi F, Lin J, et al. Self-assembled 3-D architectures of BiOBr as a visible light-driven photocatalyst. Chemistry of Materials, 2008, 20(9):2937–2941.

[17] Shu X O, Hai T Z, Dun F L, et al. Electronic structure and photocatalytic characterization of a novel photocatalyst $AgAlO_2$. Journal of Physical Chemistry B, 2006, 110(24): 11677–11682.

[18] Xu D, Cao S, Zhang J, et al. Effects of the preparation method on the structure and the visible-light photocatalytic activity of Ag_2CrO_4. Beilstein Journal of Nanotechnology, 2014, 5(5):658–666.

[19] Xu C, Liu Y, Huang B, et al. Preparation, characterization, and photocatalytic properties of silver carbonate. Applied Surface Science, 2011, 257(20):8732–8736.

[20] Peng J, Fan H, Zhang B, et al. Enhanced photocatalytic activity of β-$AgVO_3$ nanowires loaded with Ag nanoparticles under visible light irradiation. Separation & Purification Technology, 2013, 109(109):107–110.

[21] Zhiguo Y, Jinhua Y, Naoki K, et al. An orthophosphate semiconductor with photooxidation properties under visible-light irradiation. Nature Materials, 2010, 9(7):559–564.

[22] Lu X, Yu Q, Wang K, et al. Synthesis, characterization and gas sensing properties of flowerlike In_2O_3 composed of microrods. Crystal Research & Technology, 2010, 45(5): 557–561.

[23] Tang J, Zou Z, Yin J, et al. Photocatalytic degradation of methylene blue on $CaIn_2O_4$ under visible light irradiation. Chemical Physics Letters, 2003, 382:175–179.

[24] Ye J, Zou Z, Oshikiri M, et al. A novel hydrogen-evolving photocatalyst $InVO_4$ active under visible light irradiation. Chemical Physics Letters, 2002, 356(3):221–226.

[25] Fu X, Wang X, Chen Z, et al. Photocatalytic performance of tetragonal and cubic β-In_2S_3 for the water splitting under visible light irradiation. Applied Catalysis B Environmental, 2010, 95(3):393–399.

[26] Yan S C, Luo W J, Li Z S, et al. Progress in research of novel photocatalytic materials. Online Journal, 2010, 29(1):1–9. (In Chinese)

[27] Epifani M, Siciliano P, Gurlo A, et al. Ambient pressure synthesis of corundum-type In_2O_3. Journal of the American Chemical Society, 2004, 126:4078–4079.

[28] Yu D, Wang D, Qian Y. Synthesis of metastable hexagonal In_2O_3 nanocrystals by a precursor-dehydration route under ambient pressure. Journal of Solid State Chemistry, 2004, 177(4–5):1230–1234.

[29] Huang J, Gao L. Synthesis and characterization of porous single-crystal-like In$_2$O$_3$ nanostructures via a solvothermal-annealing route. Journal of the American Ceramic Society, 2006, 89(2):724–727.

[30] Lee C H, Kim M, Kim T, et al. Ambient pressure syntheses of size-controlled corundum-type In$_2$O$_3$ nanocubes. Journal of the American Chemical Society, 2006, 24(2):105–112.

[31] Dong H X, Yang H Q, Yin W Y, et al. Controlled synthesis of octahedrons, nanobelts, dentate nanowires and nanocrystal chains of In$_2$O$_3$. Acta Chimica Sinica, 2007, 65(22): 2611–2617. (In Chinese)

[32] Reyes-Gil K R, Reyes-García E A, Raftery D. Nitrogen-doped In$_2$O$_3$ thin film electrodes for photocatalytic water splitting. Journal of Physical Chemistry, 2007, 111(39): 14579–14588.

[33] Li X, Lv N, Liang S, et al. Synthesis of In$_2$O$_3$/CuO heterojunctions and their photocatalytic activity under visible light irradiation. Chinese Journal of Luminescence, 2014, 35(6):695–700. (In Chinese)

[34] Chakraborty A K, Masudur R M, Emran H M, et al. Preparation of WO$_3$/TiO$_2$/In$_2$O$_3$ composite structures and their enhanced photocatalytic activity under visible light irradiation. Reaction Kinetics Mechanisms & Catalysis, 2014, 111(1):371–382.

[35] Wang Z L, Pan Z W, Dai Z R. Structures of oxide nanobelts and nanowires. Microscopy & Microanalysis the Official Journal of Microscopy Society of America Microbeam Analysis Society Microscopical Society of Canada, 2002, 8(6):467–474.

[36] Yang H F, Shi Q H, Tian B Z, et al. One-step nanocasting synthesis of highly ordered single crystalline indium oxide nanowire arrays from mesostructured frameworks. Journal of the American Chemical Society, 2003, 125(16):4724–4725.

[37] Li C, Zhang D, Han S, et al. Diameter-controlled growth of single-crystalline In$_2$O$_3$ nanowires and their electronic properties. Advanced Materials, 2003, 15(2):143–146.

[38] Kim H W, Kim N H, Lee C. An MOCVD route to In$_2$O$_3$ one-dimensional materials with novel morphologies. Applied Physics A, 2005, 81(6):1135–1138.

[39] Liu Q, Lu W, Ma A, et al. Study of quasi-monodisperse In$_2$O$_3$ nanocrystals: synthesis and optical determination. Journal of the American Chemical Society, 2005, 127(15): 5276–5277.

[40] Lu X, Yu Q, Wang K, et al. Synthesis, characterization and gas sensing properties of flowerlike In$_2$O$_3$ composed of microrods. Crystal Research & Technology, 2010, 45(5): 557–561.

[41] Yong L, Chim W K. Highly ordered arrays of metal/semiconductor core–shell nanoparticles with tunable nanostructures and photoluminescence. Journal of the American Chemical Society, 2005, 36(18):1487–1492.

[42] Wang C, Chen D, Jiao X, et al. Lotus-root-like In_2O_3 nanostructures: fabrication, characterization, and photoluminescence properties. Journal of Physical Chemistry C, 2007, 111(36):13398–13403.

[43] Jun Y, Cui K L, Zhen L W, et al. $In(OH)_3$ and In_2O_3 nanorod bundles and spheres: microemulsion-mediated hydrothermal synthesis and luminescence properties. Inorganic Chemistry, 2006, 45(22):8973–8979.

[44] Yan Y, Cai F, Song Y, et al. $InVO_4$ nanocrystal photocatalysts: microwave-assisted synthesis and size-dependent activities of hydrogen production from water splitting under visible light. Chemical Engineering Journal, 2013, 233(11):1–7.

[45] Song L, Liu S, Lu Q, et al. Fabrication and characterization of electrospun orthorhombic $InVO_4$ nanofibers. Applied Surface Science, 2012, 258(8):3789–3794.

[46] Zou Z, Ye J, Arakawa H. Photophysical and photocatalytic properties of $InMO_4$ (M=Nb^{5+}, Ta^{5+}) under visible light irradiation. Materials Research Bulletin, 2001, 36(7): 1185–1193.

[47] Yan M, Yan Y, Wang C, et al. Ni^{2+} doped $InVO_4$ nanocrystals: one-pot microwave-assisted synthesis and enhanced photocatalytic O_2 production activity under visible-light. Materials Letters, 2014, 121(15):215–218.

[48] Shi W, Guo F, Chen J, et al. Hydrothermal synthesis of $InVO_4$/graphitic carbon nitride heterojunctions and excellent visible-light-driven photocatalytic performance for Rhodamine B. Journal of Alloys and Compounds, 2014, 612:143–148.

[49] Zhang X, Quan X, Chen S, et al. Constructing graphene/$InNbO_4$ composite with excellent absorptivity and charge separation performance for enhanced visible-light-driven photocatalytic ability. Applied Catalysis B Environmental, 2011, 105(105):237–242.

[50] Yan Y, Cai F, Song Y, Shi W. $InVO_4$ nanocrystal photocatalysts: microwave-assisted synthesis and size-dependent activities of hydrogen production from water splitting under visible light. Chemical Engineering Journal, 2013, 233(11):1–7.

[51] Hu B, Cai F, Chen T, et al. Hydrothermal synthesis g-C_3N_4/nano-$InVO_4$ nanocomposites and enhanced photocatalytic activity for hydrogen production under visible light irradiation. ACS Applied Materials & Interfaces, 2015, 7(33):18247–18256.

[52] Ye J, Zou Z, Oshikiri M, et al. A novel hydrogen-evolving photocatalyst $InVO_4$ active under visible light irradiation. Chemical Physics Letters, 2002, 356(3):221–226.

[53] Xiao G, Wang X, Li D, et al. $InVO_4$-sensitized TiO_2 photocatalysts for efficient air purification with visible light. Journal of Photochemistry & Photobiology A Chemistry, 2008, 193(2):213–221.

[54] Xu L, Sang L, Ma C, et al. Preparation of mesoporous $InVO_4$ photocatalyst and its photocatalytic performance for water splitting. Chinese Journal of Catalysis, 2006, 27(2):100–102. (In Chinese)

[55] Wang J, Nonami T. Photocatalytic activity for methylene blue decomposition of $NaInO_2$ with a layered structure. Journal of Materials Science, 2004, 39(20):6367–6370.

[56] Lekse J W, Haycock B J, Lewis J P, et al. The effect of electronic structure changes in $NaInO_2$ and $NaIn_{0.9}Fe_{0.1}O_2$ on the photo reduction of methylene blue. Journal of Materials Chemistry A, 2014, 24(24):9331–9337.

[57] Sato J, Saito N, Nishiyama H, et al. New photocatalyst group for water decomposition of RuO_2 loaded p-block metal (In, Sn, and Sb) oxides with d10 configuration. Journal of Physical Chemistry B, 2001, 105(26):6061–6063.

[58] Tang J, Zou Z, Katagiri M, et al. Photocatalytic degradation of MB on MIn_2O_4 (M=alkali earth metal) under visible light: effects of crystal and electronic structure on the photocatalytic activity. Catalysis Today, 2004, 93–95:885–889.

[59] Chen X, Shen S, Guo L, et al. Semiconductor-based photocatalytic hydrogen generation. Chemical Reviews, 2010, 110:6503–6570.

[60] Selvaraj R, Selvaraj V, Cheuk W T, et al. Self-assembled mesoporous hierarchical-like In_2S_3 hollow microspheres composed of nanofibers and nanosheets and their photocatalytic activity. Langmuir, 2011, 27(9):5534–5541.

[61] Liu G, Jiao X, Qin Z, et al. Solvothermal preparation and visible photocatalytic activity of polycrystalline β-In_2S_3 nanotubes. Crystengcomm, 2010, 1:182–187.

[62] Xing C, Wu Z, Jiang D, et al. Hydrothermal synthesis of In_2S_3/g-C_3N_4 heterojunctions with enhanced photocatalytic activity. Journal of Colloid & Interface Science, 2014, 433(11):9–15.

[63] Fu X, Wang X, Chen Z, et al. Photocatalytic performance of tetragonal and cubic β-In_2S_3 for the water splitting under visible light irradiation. Applied Catalysis B Environmental, 2010, 95(3):393–399.

[64] Xie M, Dai X, Meng S, et al. Selective oxidation of aromatic alcohols to corresponding aromatic aldehydes using In_2S_3 microsphere catalyst under visible light irradiation. Chemical Engineering Journal, 2014, 245(6):107–116.

[65] Afzaal M, Malik M A, O'Brien P. Indium sulfide nanorods from single-source precursor. Chemical Communications, 2004, 3(3):334–335.

[66] Liu G, Jiao X, Qin Z, Chen D. Solvothermal preparation and visible photocatalytic activity of polycrystalline β-In_2S_3 nanotubes. Crystengcomm, 2010, 1:182–187.

[67] Hyun P K, Kwonho J, Uk S S. Synthesis, optical properties, and self-assembly of ultrathin hexagonal In_2S_3 nanoplates. Angewandte Chemie, 2006, 45(28):4608–4612.

[68] Chen L, Zhang Z, Wang W. Self-assembled porous 3D flowerlike β-In$_2$S$_3$ structures: synthesis, characterization, and optical properties. Journal of Physical Chemistry C, 2008, 112(11):4117–4123.

[69] Zhao P, Huang T, Huang K. Fabrication of indium sulfide hollow spheres and their conversion to indium oxide hollow spheres consisting of multipore nanoflakes. Journal of Physical Chemistry C, 2007, 111(35):12890–12897.

[70] Datta A, Gorai S, Ganguli D, et al. Surfactant assisted synthesis of In$_2$S$_3$ dendrites and their characterization. Materials Chemistry & Physics, 2007, 102(2):195–200.

[71] Lei Z, You W, Liu M, et al. Photocatalytic water reduction under visible light on a novel ZnIn$_2$S$_4$ catalyst synthesized by hydrothermal method. Chemical Communications, 2003, 17(17):2142–2143.

[72] Yong J C, Shun W H, Wen J L, et al. Controlled syntheses of cubic and hexagonal ZnIn$_2$S$_4$ nanostructures with different visible-light photocatalytic performance. Dalton Transactions, 2011, 40(11):2607–2613.

[73] Yuan W H, Xia Z L, Li L, et al. Preparation and photocatalytic performance of N-doped ZnIn$_2$S$_4$ photocatalysts under visible light illumination. Journal of Functional Materials, 2014, 45(12):12117–12121. (In Chinese)

[74] Shen S, Zhao L, Zhou Z, et al. Enhanced photocatalytic hydrogen evolution over Cu-doped ZnIn$_2$S$_4$ under visible light irradiation. Journal of Physical Chemistry C, 2008, 112(41):16148–16155.

[75] Sriram M A, McMichael P H, Waghray A, et al. Chemical synthesis of the high-pressure cubic-spinel phase of ZnIn$_2$S$_4$. Journal of Materials Science, 1998, 33(17):4333–4339.

[76] Fang F, Chen L, Chen Y, et al. Synthesis and photocatalysis of ZnIn$_2$S$_4$ nano/micropeony. Journal of Physical Chemistry C, 2010, 114(6):2393–2397.

[77] Lei Z, You W, Liu M, et al. Photocatalytic water reduction under visible light on a novel ZnIn$_2$S$_4$ catalyst synthesized by hydrothermal method. Chemical Communications, 2003, 17(17):2142–2143.

[78] Shen S, Zhao L, Guan X, et al. Improving visible-light photocatalytic activity for hydrogen evolution over ZnIn$_2$S$_4$: a case study of alkaline-earth metal doping. Journal of Physics & Chemistry of Solids, 2012, 73(1):79–83.

[79] Lappe F, Niggli A, Nitsche R, et al. The crystal structure of In$_2$ZnS$_4$. Zeitschrift für Kristallographie - Crystalline Materials. DOI: 10.1524/zkri.1962.117.16.146, 1962, 117:146–152.

[80] Liang S, Peiqun Y, Yumei D. Synthesis and photocatalytic performance of ZnIn$_2$S$_4$ nanotubes and nanowires. Langmuir, 2013, 29(41):12818–12822.

[81] Bhirud A, Chaudhari N, Nikam L, et al. Surfactant tunable hierarchical nanostructures of $CdIn_2S_4$ and their photohydrogen production under solar light. International Journal of Hydrogen Energy, 2011, 36(18):11628–11639.

[82] Mu J, Wei Q, Yao P, et al. Facile preparation and visible light photocatalytic activity of $CdIn_2S_4$ monodispersed spherical particles. Journal of Alloys & Compounds, 2012, 513(6):506–509.

[83] Aguilera M L A, Hernández J R A, Trujillo M A G, et al. Photoluminescence studies of p-type chalcopyrite $AgInS_2$:Sn. Solar Energy Materials & Solar Cells, 2007, 91(s 15–16): 1483–1487.

[84] Aguilera M L A, Ortega-López M, Resendiz V M S, et al. Some physical properties of chalcopyrite and orthorhombic $AgInS_2$ thin films prepared by spray pyrolysis. Materials Science & Engineering B, 2003, 102(s 1–3):380–384.

[85] Li X, Wang L, Wei D, et al. One-pot synthesis and visible light photocatalytic activity of monodispersed $AgIn_5S_8$ microspheres. Materials Research Bulletin, 2013, 48(2):286–289.

[86] Zhang W, Li D, Chen Z, et al. Microwave hydrothermal synthesis of $AgInS_2$ with visible light photocatalytic activity. Materials Research Bulletin, 2011, 46(7):975–982.

[87] Zhang W, Li D, Sun M, et al. Microwave hydrothermal synthesis and photocatalytic activity of $AgIn_5S_8$ for the degradation of dye. Journal of Solid State Chemistry, 2010, 183(10):2466–2474.

[88] Kudo A, Nagane A, Tsuji I, et al. H_2 evolution from aqueous potassium sulfite solutions under visible light irradiation over a novel sulfide photocatalyst $NaInS_2$ with a layered Structure. Chemistry Letters, 2002, 31:882–883.

[89] Gao Y, Zhai X, Zhang Y, et al. Self-assembled cabbage-like $NaInS_2$ microstructures with efficient visible light photocatalytic performance. Journal of Solid State Chemistry France, 2013, 203(7):44–50.

[90] Tsuji I, Kato H, Prof A K. Visible-light-induced H_2 evolution from an aqueous solution containing sulfide and sulfite over a ZnS-$CuInS_2$-$AgInS_2$ solid-solution photocatalyst. Angewandte Chemie, 2005, 44(34):3565–3568.

[91] Tsuji I, Kato H, Kudo A. Photocatalytic hydrogen evolution on ZnS–$CuInS_2$–$AgInS_2$ solid solution photocatalysts with wide visible light absorption bands. Chemistry of Materials, 2006, 18(7):1969–1975.

[92] Zhang X, Du Y, Zhou Z, et al. A simplified method for synthesis of band-structure-controlled $(CuIn)_xZn_{2(1-x)}S_2$ solid solution photocatalysts with high activity of photocatalytic H_2 evolution under visible-light irradiation. International Journal of Hydrogen Energy, 2010, 35(8):3313–3321.

[93] Shen S, Zhao L, Zhou Z, et al. Enhanced photocatalytic hydrogen evolution over Cu-doped $ZnIn_2S_4$ under visible light irradiation. Journal of Physical Chemistry C, 2008, 112(41):16148–16155.

[94] Ma G J, Lei Z B, Yan H J, et al. Photocatalytic hydrogen production on $CuInS_2$-ZnS solid solution prepared by solvothermal method. Chinese Journal of Catalysis, 2009, 30(1): 73–77. (In Chinese)

[95] Li Y, Chen G, Zhou C, et al. A simple template-free synthesis of nanoporous ZnS–In_2S_3–Ag_2S solid solutions for highly efficient photocatalytic H_2 evolution under visible light. Chemical Communications, 2009, 15:2020–2022.

[96] Li Y X, Chen G, Wang Q, et al. Hierarchical ZnS-In_2S_3-CuS nanospheres with nanoporous structure: facile synthesis, growth mechanism, and excellent photocatalytic activity. Advanced Functional Materials, 2010, 20(19):3390–3398.

[97] Tsuji T, Kato H, Kobyashi H, et al. Photocatalytic H_2 evolution reaction from aqueous solutions over band structure-controlled $(AgIn)_xZn_{2(1-x)}S_2$ solid solution photocatalysts with visible-light response and their surface nanostructures. Journal of the American Chemical Society, 2004, 126(41):13406–13413.

[98] Zhang K, Jing D W, Xing C J, et al. Research on the preparation of $(CuAg)_xIn_{2x}Zn_{2(1-2x)}S_2$ solid solution photocatalysts. International Symposium on Multiphase Flow, 2010, 1207:1066–1069.

[99] Lei Z, Liu M, You W, et al. Sulfur-substituted and zinc-doped $In(OH)_3$: a new class of catalyst for photocatalytic H_2 production from water under visible light illumination. Journal of Catalysis, 2008, 237(2):322–329.

[100] Song Y, Xu L, Shi W, et al. A facile in situ fabrication and visible-light-response photocatalytic properties of porous carbon sphere/InOOH nanocomposites. Journal of Nanoparticle Research, 2014, 2295(3):452–457.

[101] Ge S, Wang B, Lin J, et al. C, N-co doped InOOH microspheres: one-pot synthesis, growth mechanism and visible light photocatalysis. Crystengcomm, 2012, 4(4):721–728.

[102] Matsuoka T, Nakao M. Mysterious material InN in nitride semiconductors – what's the bandgap energy and its application? 2007 IEEE 19th International Conference on Indium Phosphide & Related Materials, 2007:372–375.